Journal of Molecular Structure 1020 (2012) 6–15

Contents lists available at SciVerse ScienceDirect

Journal of Molecular Structure

journal homepage: www.elsevier.com/locate/molstruc

Synthesis, characterization, molecular modeling and antioxidant activity of (1E,5E)-1,5-bis(1-(pyridin-2-yl)ethylidene)carbonohydrazide (H_2APC) and its zinc(II), cadmium(II) and mercury(II) complexes

O.A. El-Gammal *, G.M. Abu El-Reash, S.E. Ghazy, A.H. Radwan

Department of Chemistry, Faculty of Science, Mansoura University, P.O. Box 70, Mansoura, Egypt

ARTICLE INFO

Article history:
Received 25 March 2012
Accepted 10 April 2012
Available online 18 April 2012

Keywords:
Carbohydrazone
Spectral characterization
Thermal analysis
DFT and ABTS
DPPH-activity

ABSTRACT

A new series of Zn(II), Cd(II) and Hg(II) complexes of (1E,5E)-1,5-bis(1-(pyridin-2-yl)ethylidene)carbonohydrazide (H_2APC) have been prepared and characterized by elemental analyses, spectral (IR, UV–visible, mass and ^{1}H NMR) as well as magnetic and thermal measurements. The data revealed that the ligand acts a monobasic hexadentate, neutral tri- and monodentate in Zn(II), Cd(II) and Hg(II) complexes, respectively. An octahedral geometry is proposed for Zn(II) complex, a trigonal bi-pyramid for Cd(II) complex and a tetrahedral one for Hg(II) complex. The bond length, bond angle, HOMO, LUMO and charges on the atoms have been calculated to confirm the geometry of the ligand and the investigated complexes using material studio program. Kinetic parameters were determined for each thermal degradation stage of some complexes using Coats–Redfern and Horowitz–Metzger methods. The antioxidant, anti-hemolytic, and cytotoxic activities of the compounds have been screened. H_2APC showed moderate antioxidant activity using ABTS and DPPH methods. With respect to erythrocyte hemolysis and in vitro Ehrlich ascites assay, H_2APC exhibited the potent antioxidative activity followed by Cd(II) and Zn(II) complexes while Hg(II) complex showed very weak activity.

1. Introduction

Carbohydrazones have been found to be one of the most fascinating subjects in the field of coordination chemistry due to their well known physiological activity, coordinative capability and applications in analytical chemistry [1–4]. Ligands derived from substituted carbohydrazone have played an important part in revealing the preferred coordination geometries of metal complexes and have valuable contribution in the coordination chemistry due to their preparative accessibility, diversity and structural variability. The carbohydrazones and their complexes with transition metal ions have been well documented in the literature as good therapeutic, antimicrobial, anticonvulsant, pharmacological and catalytic agents [5–7]. The ligands that contain an amidic bond are capable of keto–enol tautomerism and coordinated to a metal ion in neutral or deprotonated form as quinquedentates, via pyridine nitrogen, hydrazone nitrogen and carbonyl oxygen atoms. However, the coordination behavior of ligands depends on the metal ion, the pH of the medium, the reaction conditions and the nature of the hydrazones [8–14]. The present work aims to investigate the chelating properties of (1E,5E)-1,5-bis(1-(pyridin-2-yl)ethylidene)carbonohydrazide (H_2APC) towards Zn(II), Cd(II) and Hg(II) metal ions in more details, including structural elucidation, thermal behavior and molecular modeling of both ligand and its complexes. Also, the antioxidant activity evaluated using DPPH· (2,2′-diphenyl-1-picrylhydrazyl radical), ABTS (2-azino-bis(3-ethylbenzthiazoline)-6-sulfonic acid) and anti-hemolytic as well as cytotoxic activities of the compounds have been discussed.

2. Experimental

2.1. Instrumentation and materials

All the chemicals were purchased from Aldrich and Fluka and used without further purification. Elemental analyses (C, H, N) were performed with a Perkin–Elmer 2400 series II analyzer. Molar conductance values (10^{-3} mol l^{-1}) of the complexes in DMF were measured using a Tacussel conductivity bridge model CD6NG. IR spectra (4000–400 cm^{-1}) for KBr discs were recorded on a Mattson 5000 FTIR spectrophotometer. Electronic spectra were recorded on a Unicam UV–Vis spectrophotometer UV2. Magnetic susceptibilities were measured with a Sherwood scientific magnetic susceptibility balance at 298 K. ^{1}H NMR measurements in d_6-DMSO at room temperature were carried out on a Varian Gemini WM-300 MHz spectrometer at the Microanalytical Unit, Cairo University. Thermogravimetric measurements (TGA, DTA, 20–1000 °C) were recorded

* Corresponding author. Tel.: +20 126712958.
E-mail address: olaelgammal@hotmail.com (O.A. El-Gammal).

0022-2860/$ - see front matter © 2012 Elsevier B.V. All rights reserved.
http://dx.doi.org/10.1016/j.molstruc.2012.04.029

on a DTG-50 Shimadzu thermogravimetric analyzer at a heating rate of 15 °C/min and nitrogen flow rate of 20 ml/min.

2.2. Synthesis of (1E,5E)-1,5-bis(1-(pyridin-2-l)ethylidene) carbonohydrazide (H_2APC)

The carbohydrazone was synthesized by refluxing 2-acetylpyridine (0.30 ml, 2.7 mmol) and carbonohydrazide (0.10 g, 1.1 mmol) in 2:1 M ratio in hot ethanol with adding few drops of glacial acetic acid to the reaction mixture. The solution was heated for 4 h and on cooling a white solid was precipitated. The product was recrystallized from absolute ethanol as colorless needles, yield 80%. The compound was checked by its m.p., (decomp. at 186 °C), TLC, IR and ^{1}H NMR spectra.

2.3. Synthesis of complexes

2.3.1. Synthesis of Cd(II), Hg(II) complexes

A hot ethanolic solution of the respective metal chloride (1.0 mmol) was added to hot ethanolic solution of (H_2APC) (0.296 g, 1.0 mmol). The resultant mixture was heated under reflux for 6 h. Pale yellow precipitates that formed were filtered off, washed with ethanol followed by diethyl ether and dried in a vacuum desiccator over anhydrous $CaCl_2$. The complexes are stable in air. Hg(II) complex is insoluble in either polar or non-polar solvents and vice versa in case of Cd(II) complex which is readily soluble.

2.3.2. Synthesis of Zn(II) complex

A hot ethanolic solution of the zinc acetate (1.0 mmol) was added to hot ethanolic solution of (H_2APC) (0.296 g, 1.0 mmol). The resultant mixture was heated under reflux for 8 h. The deep red solution that obtained was evaporated to quarter of the volume and treated with diethyl ether forming orange precipitate. The product was dried in a vacuum desiccator over anhydrous $CaCl_2$. The complex is stable and readily soluble in polar and non-polar solvents.

2.4. Biological studies

2.4.1. Anti-oxidant activity screening

The antioxidant activity assay [15] employed is a technique depending on measuring the consumption of stable free radicals i.e. evaluate the free radical scavenging activity of the investigated component. The methodology assumes that the consumption of the stable free radical (X') will be determined by reactions as follows:

$$X' + YH \rightarrow XH + Y'$$

The rate and/or the extent of the process measured in terms of the decrease in X' concentration, would be related to the ability of the added compounds to trap free radicals. The decrease in color intensity of the free radical solution due to scavenging of the free radical by the antioxidant material is measured colorimetry at a specific wavelength. The assay employs the radical cation derived from 2,2′-azino-bis(3-ethyl-benzthiazoline-6-sulfonic acid) (ABTS) or diphenylpicrylhydrazyl (DPPH) as stable free radicals to assess antioxidant and extracts. The Inhibition percent of the free radical DPPH or ABTS was calculated according to the equation:

$$I\% = (A_{blank} - A_{sample})/(A_{blank}) \times 100$$

where A_{blank} is the absorbance of the control reaction (containing all reagents except the test compound), and A_{sample} is the absorbance of the test sample.

2.4.1.1. Antioxidant activity screening assay DPPH method. The hydrogen atom or electron donation ability of the corresponding compounds was measured from the bleaching of purple colored of the methanolic solution of DPPH. This spectrophotometric assay uses the stable radical diphenylpicrylhydrazyl (DPPH) as a reagent [16,17]. Different concentrations of the chemical compounds were dissolved in methanol to obtain final concentration ranged from 6.25 to 200 mg/ml to determine IC_{50} (concentration make 50% inhibition of DPPH color). Fifty microliters of various sample concentrations were added to 5 ml of 0.004% methanolic solution of DPPH. After 60 min of incubation at dark, the absorbance was read against a blank at 517 nm.

2.4.1.2. Antioxidant activity screening assay ABTS method. The reaction mixture (negative control) consists of 2 ml of 2,2′-azino-bis-(3-ethyl-benzthiazoline-6-sulfonic acid) (ABTS) solution (60 μl) and 3 ml of MnO_2 solution (25 mg/ml), all prepared in phosphate buffer (pH = 7) [18–20]. The mixture was shaken, centrifuged and filtered to remove the excess oxide. The absorbance ($A_{control}$) of the resulting green–blue solution ($ABTS^+$ radical solution) was recorded at λ_{max} = 734 nm. The absorbance (A_{test}) was measured upon the addition of 20 μl of 1 mg/ml solution of the test sample under investigation in spectroscopic grade MeOH/buffer (1:1 v/v) to the ABTS solution. Ascorbic acid 20 μl (2 ml) solution was used as standard antioxidant (positive control). Blank sample was run using solvent without ABTS. The decrease in absorbance is expressed as % inhibition.

2.4.1.3. Antioxidant activity screening assay for erythrocyte hemolysis. The blood was obtained from rats by cardiac puncture and collected in heparinized tubes. Erythrocytes were separated from plasma and the buffy coat was washed three times with 10 volumes of 0.15 M NaCl. During the last wash, the erythrocytes were centrifuged at 2500 rev./min for 10 min to obtain a constantly packed cell preparation. Erythrocyte hemolysis was mediated by peroxyl radicals in this assay system [21]. A 10% suspension of erythrocytes in phosphate buffered saline pH 7.4 (PBS) was added to the same volume of 200 mM AAPH solution in PBS containing samples to be tested at different concentrations. The reaction mixture was shaken gently while being incubated at 37 °C for 2 h. The reaction mixture was then removed, diluted with eight volumes of PBS and centrifuged at 1500*g* for 10 min. The absorbance of the supernatant was read at 540 nm. Similarly, the reaction mixture was treated with eight volumes of distilled water to achieve complete hemolysis, and the absorbance of the supernatant obtained after centrifugation was measured at 540 nm. The data percentage hemolysis was expressed as mean ± standard deviation. L-ascorbic acid was used as a positive control.

2.4.2. Cytotoxic activity

2.4.2.1. Ehrlich cells. Ehrlich cells (Ehrlich ascites Carcinoma, EAC) were derived from ascetic fluid from diseased mouse (the cells were purchased from National Cancer Institute, Cairo, Egypt which is a certified institute by National Medical Research Ethics Committee). DNA (Calf Thymus type1), bleomycin sulfate, butylatedhydroxyanisole (BHA), thiobarbituric acid (TBA), ethylenediaminetetraacetic acid (EDTA) and ascorbic acid were obtained from sigma. 2,20-azo-bis-(2-amidinopropane) dihydrochlorid (AAPH), 2,2′-azino-bis-3-ethylbenzthiazoline-6-sulfonic acid (ABTS) were purchased from Wako Co., USA.

2.4.2.2. Antitumor activity using Ehrlich ascites in vitro assay. Different concentrations of the tested compounds were prepared (100, 50 and 25 ml from 1 mg/ml in DMSO (<00.05%, v/v) and RPMI-1640 medium). The ascites fluid from the peritoneal cavity of the diseased mouse (contains Ehrlich cells) was aseptically aspirated.

The cells were grown partly floating and partly attached in a suspension culture in RPMI-1640 medium, supplemented with 10% fetal bovine serum. They were maintained at 37 °C in a humidified atmosphere with 5% CO_2 for 2 h. The viability of the cells determined by the microscopical examination using a hemocytometer and using trypan blue stain (stains only the dead cells) [22,23].

2.5. Molecular modeling

We performed cluster calculations using DMOL^3 program [24] in Materials Studio package [25], which is designed for the realization of large scale density functional theory (DFT) calculations. DFT semi-core pseudopods calculations (dspp) were performed with the double numerica basis sets plus polarization functional (DNP). The DNP basis sets are of comparable quality to 6-31G Gaussian basis sets [26]. Delley et al. showed that the DNP basis sets are more accurate than Gaussian basis sets of the same size [25]. The RPBE functional [27] is so far the best exchange–correlation functional [28], based on the generalized gradient approximation (GGA), is employed to take account of the exchange and correlation effects of electrons. The geometric optimization is performed without any symmetry restriction.

3. Results and discussion

The data of elemental analysis together with some physical properties of the complexes are summarized in Table 1. The stoichiometries of the coordination adducts established by elemental analysis are confirmed by weight loss determination. The values of molar conductivity of all complexes lie in the range (1–17 Ω^{-1} cm^2 mol^{-1}) indicating their non-electrolytic nature [29].

3.1. Molecular modeling

The molecular structure along with atom numbering of (H_2APC) and its metal complexes are shown in structures 1–4. Analysis of the data in Tables 1S–8S including the bond lengths and bond angles, one can conclude the following remarks:

1. The N(3)—N(6), N(3)—C(2) and N(6)—C(7)$_{azomethine}$ bond lengths become slightly longer in complexes as the coordination takes place via N atoms of —C=N—C=N— group that is formed on deprotonation of OH group in $[Zn_2(HAPC)(OAc)_3(H_2O)_3]\cdot 3H_2O$ complex [30].
2. The C(2)—O(4) bond distance in all complexes becomes longer due to the formation of the M—O bond which makes the C—O bond weaker [31].
3. In $[Zn_2(HAPC)(OAc)_3(H_2O)_3]\cdot 3H_2O$ complex, C(8)—N(10) and C(17)—N(22) bond distances of the two pyridine rings pyridine are enlonged. This is referred to the formation of the M—O bond which makes the C—O bond weaker and forming a double bond character [32].
4. The bond angles of the hydrazine moiety of H_2APC are altered somewhat upon coordination; the largest change affects C(2)—N(3)—N(6) and O(4)—C(2)—N(3) angles which are reduced or increased on complex formation as a consequence of bonding [31].
5. The C(2)—N(3)—N(6) angle changes from 117.9° to 112.2° or 116.6° in $[Zn_2(HAPC)(OAc)_3(H_2O)_3]\cdot 3H_2O$ and $[Cd(H_2APC)Cl_2]$ complexes due to the formation of the N(13)—Zn—O(22) and N (8)—Cd—O(25) chelate ring [32].
6. The bond angles, N(10)—M(7)—Cl(23), N(10)—M(7)—Cl(24), O(25)—M(7)—N(10) and O(25)—M(7)—N(8) of 142.8, 106.1, 60.77 and 61.29 in $[Cd(H_2APC)Cl_2]$ complex indicate that the complex adopts a trigonal bipyramidal arrangement. On the other hand the bond angles in $[Zn_2(HAPC)(OAc)_3(H_2O)_3]\cdot 3H_2O$ $[Hg_2(H_2APC)_2Cl_4]$ complexes are quite near to an octahedral and tetrahedral geometries, respectively predicting sp^3 d^2 and sp^3 hybridization.
7. The complexes can be arranged according to M—N$_{azomethine}$ and M—O bond lengths as follows: Zn(23)—N(13), Zn(31)—N(12) > Cd(7)—N(10), Cd(7)—N(8) and Hg—O > Zn—O > Cd—O reflecting the great strength of the Zn—N and Hg—O bonds.
8. The lower HOMO energy values show that molecules donating electron ability is the weaker. On contrary, the higher HOMO energy implies that the molecule is a good electron donor. LUMO energy presents the ability of a molecule receiving electron [33].
9. The bond angles within the hydrazone backbone do not change significantly but the angles around the metal undergo appreciable variations upon changing the metal center [34].

3.2. IR spectra

The principle IR bands of H_2APC and its metal complexes are represented in Table 2. The IR spectrum of H_2APC (Structure 1) showed two bands at 1698 and 1679 cm^{-1} attributable to stretching vibration mode of (C=O) group [35] suggesting the existence of the ligand in syn and anti-conforms (b, c). The band observed at 1626 cm^{-1} is assignable to ν(C=N) vibration and shifted to lower wavenumber upon complexation. The ligand showed bands at 1,579,989,651 and 410 cm^{-1} are attributable to ν(C=N) pyridine stretching [36], pyridine ring breathing, in-plane-bending and out-of plane ring vibration modes [37–39], respectively. Also, the medium intensity band at 1045 cm^{-1} is attributable to ν(N—N) stretching vibration [40,41] while the band at 3207 cm^{-1} is assigned to the ν(NH) vibrational mode. The bands 3207, 3351 cm^{-1}assigned to ν(NH^a) and ν(NH^b), respectively. The ν(NH^b) appeared at higher wavenumber because the hydrogen bond with N atom of pyridine ring (Structure 1a).

Comparison of the IR spectra of H_2APC and its metal complexes (Table 2) showed that H_2APC has two modes of coordination. Firstly, as monobasic hexadentate in $[Zn_2(HAPC)(OAc)_3(H_2O)_3]\cdot 3H_2O$ complex (Structure 2) via the carbonyl oxygen (C=O) in

Table 1
Analytical and physical data of H_2APC and its metal complexes.

Compound		Color	m.p. (°C)	% Found (Calcd.)				Yield (%)
Empirical formula	(F.Wt)			M	Cl	C	H	
(H_2APC)		White	186 (decomp)	–	–	60.9 (60.80)	5.46 (5.44)	80
$C_{15}H_{16}N_6O$	(296.33)							
$Cd(H_2APC)Cl_2$		Pale yellow	270	23.44	14.93	37.63	3.42	84
$C_{15}H_{16}CdCl_2N_6O$	(479.64)			(23.6)	(14.78)	(37.56)	(3.36)	
$[Hg_2(H_2APC)_2Cl_4]$		Pale yellow	232	35.5	12.52	31.79	2.88	88
$C_{30}H_{32}Cl_4Hg_2N_{12}O_2$	(1135.7)			(35.33)	(12.49)	(31.73)	(2.84)	
$[Zn_2(HAPC)(OAc)_3(H_2O)_3](H_2O)_3$		Orange	>300	18.38	–	35.12	4.96	89
$C_{21}H_{36}N_6O_{13}Zn_2$	(711.33)			(18.5)		(35.46)	(5.1)	

Table 2
Most important IR spectral bands of H_2APC and its metal complexes.

Compound	υ(NH)	υ(C=O)	υ(C=N)	υ(C=N)$_{py}$	δ(C=N)$_{py}$	υ(C=N*)	υ(C–O) enolic	υ(M–O)	υ(M–N)
H_2APC	3207 3351	1698 1679	1616	1540	651	–	–	–	–
$[Cd(H_2APC)Cl_2]$	3212 3357	1662	1558	1525	666	–	–	500	427
$[Hg_2(H_2APC)_2Cl_4]$	3232 3326	1689	1625	1540	645	645	–	507	481
$[Zn_2(HAPC)(OAc)_3(H_2O)_3](H_2O)_3$	3310	–	1575	1550	660	1629	1197	507	425

υ(C=N*): New azomethine.

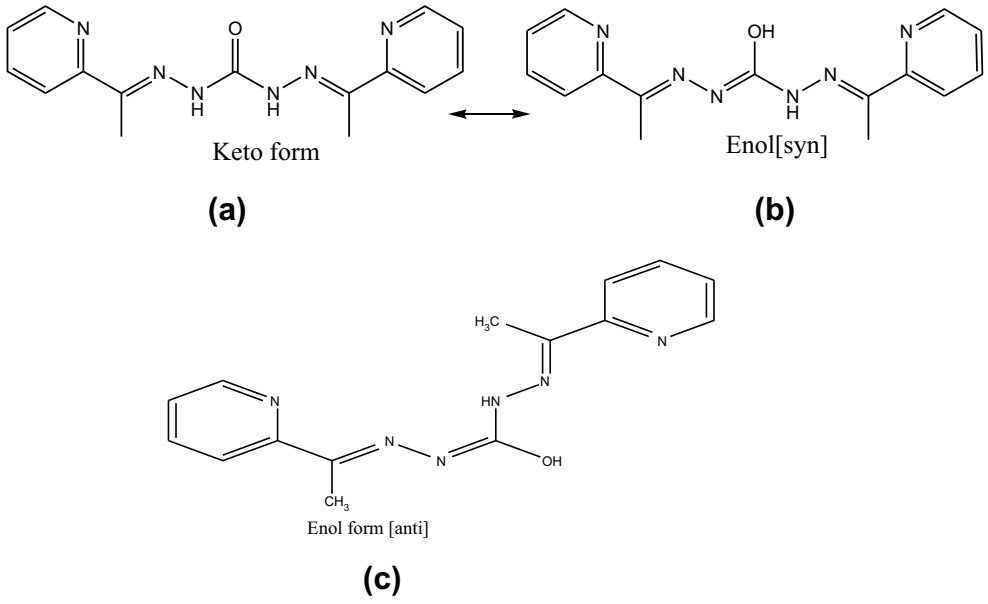

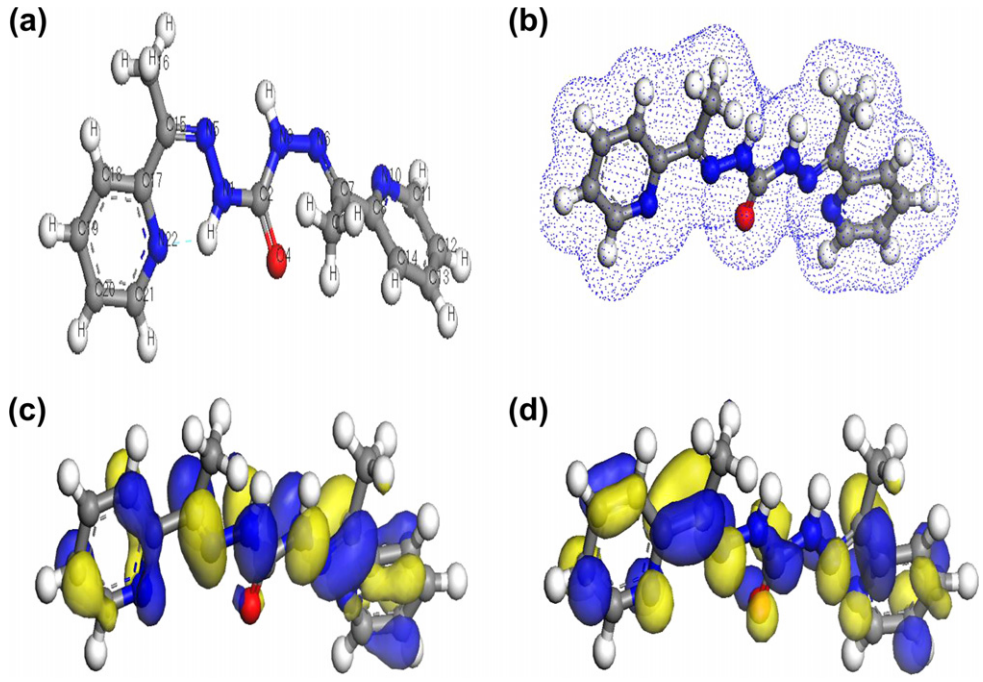

Structure 1. Molecular structure of (a) H_2APC (b) electron density of H_2APC (c) HOMO of H_2APC (d) LUMO of H_2APC.

the enol form, the two azomethine nitrogens, (C=N) that already exists and the new (C=N)* that formed on enolization and (C=N)$_{py}$ groups. This mode of chelation is confirmed by the following evidences: (i) the disappearance of bands due to ν(C=O) and ν(NH)

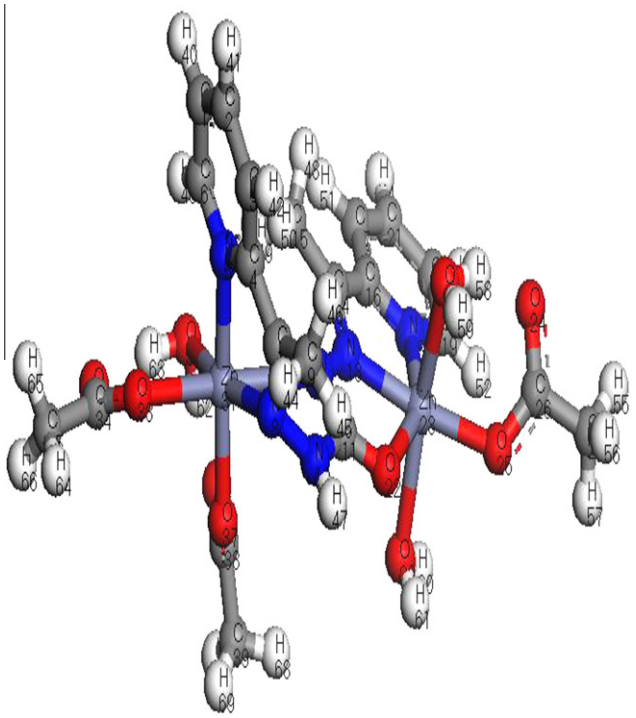

Structure 2. Molecular modeling of $[Zn_2(HAPC)(OAc)_3(H_2O)_3](H_2O)_3$.

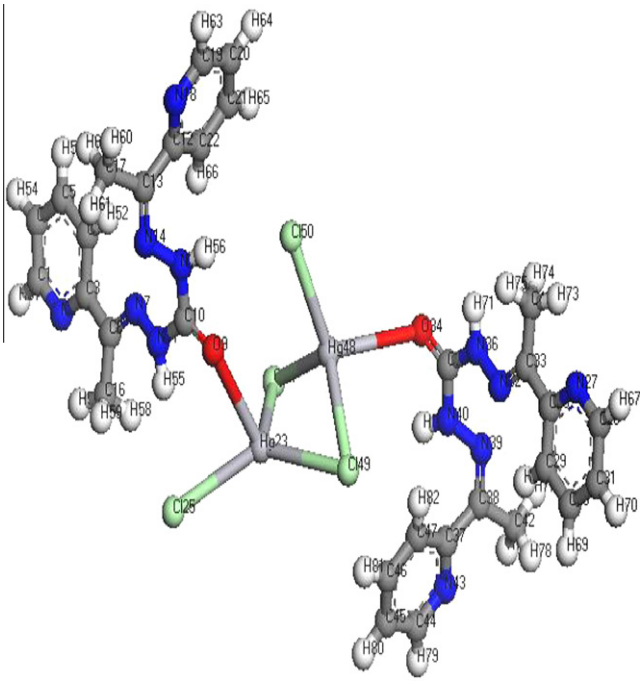

Structure 3. Molecular modeling of $[Hg_2(H_2APC)_2Cl_4]$.

modes with simultaneous appearance of new bands at 1629 and 1197 cm^{-1} assignable to ν(C=N)* and ν(C—O) modes, (ii) ν(N—N) shifts to higher wavenumber as a result of the increase in the double bond character of N—N offsetting the loss of electron density via donation to the metal ion and is a further evidence of coordination of the ligand through the azomethine nitrogen atom., (iii) the bands due to $\nu(C{=}N)_{azomethine}$, ν(C=N) pyridine and pyridine ring breathing modes shift to lower wavenumber and (iv) moreover,

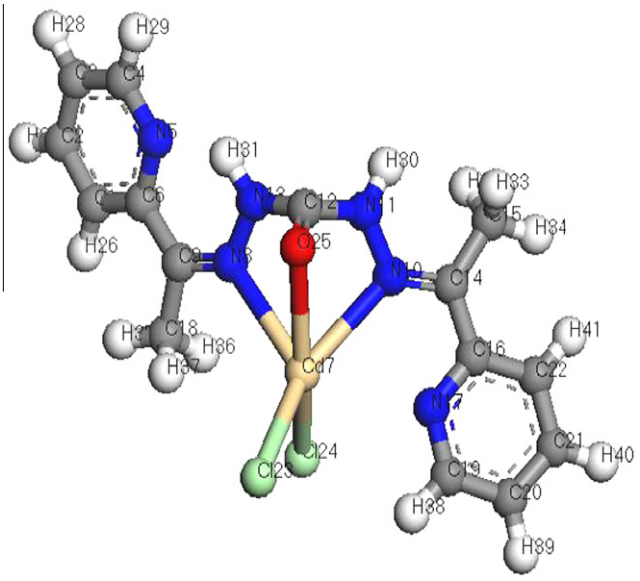

Structure 4. Molecular modeling of $[Cd((H_2APC)Cl_2]$.

the band due to pyridine ring deformation shifts to higher wavenumber is an additional evidence of coordination through (C=N) pyridine atom [42]. The broad bands observed at 1550 and 1426 cm^{-1} assignable to ν_{asym}(OCO) and ν_{sym}(OCO) vibrations, respectively with frequency difference ($\Delta\nu$ = 123 cm^{-1})confirming monodentate nature of the acetate group [43]. Secondly, H_2APC coordinates either as neutral mono-dentate as in $[Hg_2(H_2APC)_2Cl_4]$ complex (Structure 3) via the carbonyl oxygen (C=O) in the keto form as illustrated by shift of its band to lower wavenumber or as neutral tridentate manner through (C=O) and both azomethine nitrogen atoms in case of $[Cd(H_2APC)Cl_2]$ complex (Structure 4). This mode of coordination is supported by the shift of the stretching vibrations of both azomethine groups to lower wavenumber and shift of ν(N—N) to higher wave-number [44,45]. The suggested mode of chelation for the aforementioned complexes is also confirmed by the appearance of new bands at 500–507 and 420–427 cm^{-1} attributable to ν (M—O) [46] and ν (M—N) [47], respectively.

3.3. The ^1H NMR

The ^1H NMR spectrum of H_2APC is displayed in DMSO-d_6 solution. The signals of all hydrogen are duplicated suggesting the existence of the anti and syn configurations in solution [48]. In fact, two signals of NH protons were observed as doublet at downfield δ10.03 (anti) and 10.13 ppm (syn) which disappear upon adding D_2O. The signals at δ2.10–2.51 ppm may be equivalent to 12 protons of the four CH_3 groups. The signals due to pyridine ring protons appeared at δ: {6.687 (anti), 7.33 ppm (syn) (t, 2H, H—C12=H—C20)}, {7.36 (anti), 7.56 (syn) ppm (t, 2H, H—C13=H—C19)}, {7.85 (anti), 8.03 ppm (syn) (d, 2H, H—C14=H—C18)} and {8.57 (anti) 8.69 (syn) ppm (d, 2H, H—C11=H—C21)} [48,49]. Also, the signal at 14.3 ppm may be corresponding to enolic proton of ligand in solution. This signal supported the existence of the ligand in keto–enol form in solution which disappears upon addition of D_2O as illustrated in Structure 1. The above assumption was confirmed by the molecular modeling of H_2APC as the two isomers possessed the same binding energy (−4043.32, 4043.48 kcal/mol for anti and syn isomers, respectively).

Further evidence for deprotonation of the enolized carbonyl oxygen comes from the ^1H NMR spectrum of the diamagnetic Zn(II)

Table 3
Decomposition steps with the temperature range and weight loss for H_2APC complexes.

Compound	Decomposition step	Temperature range (°C)	Removes species	wt loss	
				% (Calcd.)	% Found
$[Cd(H_2APC)Cl_2]$	1st	264–297	$-2N_2$	11.68	11.90
	2nd	354–415	$-HCl + C_5H_5N$	23.88	24.10
	3rd	441–469	$-HCl$	7.60	7.63
	4th	555–607	$-C_5H_5N + C_3H_6$	30.06	30.30
	Residue	607–800	$-CdO$	26.80	26.07
$[Zn_2(HAPC)(OAc)_3(H_2O)_3](H_2O)_3$	1st	57–96	$-3H_2O$	7.59	8.28
	2nd	138–169	$-3H_2O$	7.59	8.12
	3rd	292–326	$-2HOAc$	16.86	16.34
	4th	398–479	$-2C_5H_5N + N_2 + HOAc$	34.28	33.80
	5th	547–589	$-CH_3CN + HCN$	9.55	9.12
	Residue	589–800	$Zn + ZnO + 2C$	23.99	24.34

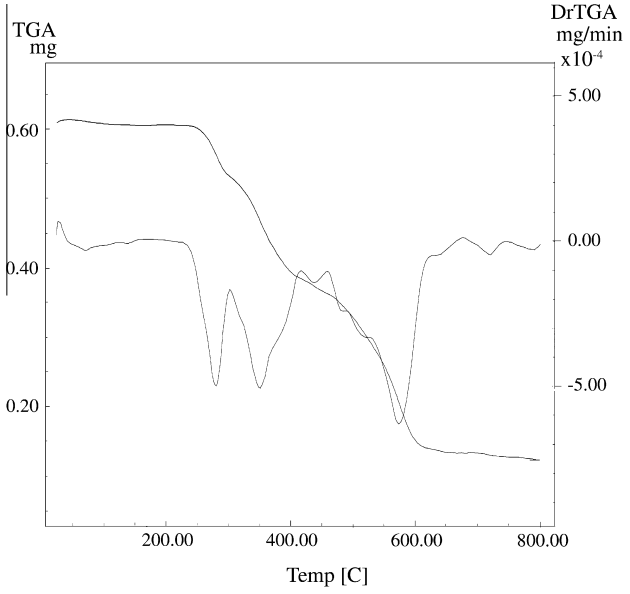

Fig. 1. Thermal analysis curves (TGA, DTG) of $[Cd(H_2APC)Cl_2]$.

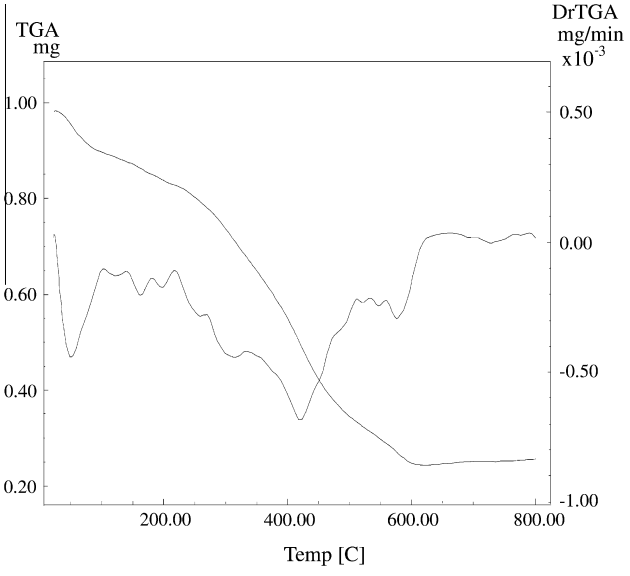

Fig. 2. Thermal analysis curves (TGA, DTG) of $[Zn_2(HAPC)(OAc)_3(H_2O)_3](H_2O)_3$.

complex, emphasizing the lack of the signals due to the first NH proton while the second NH signal shifted to high field as involved in hydrogen bonding with N of the pyridine ring and overlapped with the signals of pyridine protons. The appearance of multiplet at 3.57–3.41 ppm is due to the CH_3CH_2 protons of the acetate.

3.4. Electronic spectra

The electronic spectrum of the ligand and its complexes was displayed in DMF or Nujol mull. The tentative assignments of the significant spectral absorption bands are given in Table 3. The electronic spectra of the complexes are dominated by intense intra-ligand charge transfer bands. The spectrum f the ligand shows an intense absorption band at 36,496–35,971 cm^{-1} region assigned to $\pi \rightarrow \pi^*$ transition of pyridine rings [50]. A red shift is observed for this transition in the spectrum of $[Zn_2(HAPC)(OAc)_3(H_2O)_3]\cdot 3H_2O$ complex as a result of coordination of the nitrogen of the pyridine ring [49]. Another intense absorption band in the region 33,557 cm^{-1} assigned to $\pi \rightarrow \pi^*$ of C=N group which shifts in all complexes toward higher frequencies, supporting the coordination of the hydrazone via azomethine nitrogen atom. A third intense band is observed in the 25,907–28,089 cm^{-1} region assignable to $n \rightarrow \pi^*$ transition of carbonyl group [49]. In complexes, this band is shifted by ~150–409 cm^{-1}.

Owing to the deep orange color of $[Zn_2(HAPC)(OAc)_3(H_2O)_3]\cdot 3H_2O$ complex, its spectrum in Nujol mull was displayed. The spectrum exhibited a moderately intense broad bands in the region 24,876–19,084 cm^{-1} may be due to L–M charge transfer. Except this, the complex showed no appreciable absorptions in the region below 190,84, in accordance with d^{10} electronic configuration of Zn(II) ion.

3.5. Thermogravimetric studies

The stages of decomposition, temperature range, decomposition product as well as the weight loss percentages of Cd(II) and Zn(II) complexes are given in Table 3. Figs. 1 and 2 shows the TGA curves of some metal complexes. The experimental weight loss values are in good agreement with the calculated values. The final decomposition product was identified by the conventional chemical analysis method. $[Zn_2(HAPC)(OAc)_3(H_2O)_3]\cdot 3H_2O$ complex is chosen as a representative example since it contains both types *viz.* water of coordination and water of crystallization. In the TG thermogram of this complex, the first stage at 57–96 °C with weight loss of 8.28 (Calcd. 7.59%) is corresponding to the loss of the three lattice water molecules. The second step with weight loss of 8.12 (Calcd. 7.59%) at 138–169 °C is attributed to the elimination of three coordinated water molecules. The third step at 292–326 °C with weight loss of 16.34 (Calcd. 16.86%) is referring to the removal of 2HOAc molecules. The fourth step corresponds to the elimination of $2C_5H_5N + N_2 + HOAc$ fragments with weight loss of 33.80 (Calcd.

Table 4
Kinetic parameters evaluated by Coats–Redfern equation for H_2APC complexes.

Complex	Peak	Mid temp (K)	E_a (kJ/mol)	A (S^{-1})	ΔH^* (kJ/mol)	ΔS^* (kJ/mol K)	ΔG^* (kJ/mol)
$[Zn_2(HAPC)(OAc)_3(H_2O)_3](H_2O)_3$	1st	349.52	8.06	5.71×10^3	35.16	−0.1743	96.08
	2nd	427.00	6.07	3.82×10^{-3}	2.52	−0.2942	128.14
	3rd	581.89	104.29	1.34×10^7	99.45	−0.1140	165.79
	4th	711.51	37.58	1.50×10^1	31.66	−0.2487	8.65
	5th	840.87	165.09	7.92×10^7	158.10	−0.1023	244.13
$[Cd(H_2APC)Cl_2]$	1st	170.18	170.18	1.95×10^{14}	165.58	0.0235	152.56
	2nd	94.60	94.60	3.82×10^5	89.13	−0.1446	184.21
	3rd	141.08	141.08	6.36×10^7	135.03	−0.1029	209.98
	4th	202.85	202.85	3.29×10^7	195.75	−0.0523	240.45

34.28%). This is followed by loss of $C_3H_4N_2$ fragment with weight loss of 9.12 (Calcd. 9.55%). The residual part is Zn + ZnO + 2C (found 24.34, Calcd. 23.99%). An inspection of the data represented in Table 4 indicates that TG thermograms displayed a high residual part for the studied complexes reflecting a higher thermal stability owing to the existence of five membered chelate rings.

3.6. Kinetic data

The kinetic and thermodynamic parameters of thermal degradation process have been calculated using Coats–Redfern and Horowitz–Metzger models [51,52]. Coats–Redfern relation is as follows:

$$\ln\left[-\frac{\ln(1-\alpha)}{T^2}\right] = \ln\left(\frac{AR}{\beta E}\right) - \frac{E}{RT} \quad (1)$$

where α represents the fraction of sample decomposed at time t, defined by:

$$\alpha = \frac{w_o - w_t}{w_o - w_\infty}$$

In which w_o, w_t and w_∞ are the weight of the sample before the degradation, at temperature t and after total conversion, respectively. T is the derivative peak temperature. β is the heating rate = dT/dt, E and A are the activation energy and the Arrhenius pre-exponential factor, respectively. A plot of $\ln[-\ln(1-\alpha)/T^2]$ versus $1/T$ gives a straight line whose slope (E/R) and the pre-exponential factor (A) can be determined from the intercept.

The Horowitz–Metzger relation [52] used to evaluate the degradation kinetics is:

$$\ln[-\ln(1-\alpha)] = \frac{E\theta}{RT_s^2} \quad (2)$$

where $\theta = T - T_s$, T_s is the DTG peak temperature, T is the temperature corresponding to weight loss wt. A straight line should be observed between $\ln[-\ln(1-\alpha)]$ and θ with a slope of E/RT_s^2. A number of pyrolysis processes can be represented as a first order reaction. Particularly, the degradation of a series of H_2APC complexes was suggested to be first order [53], therefore we assume $n = 1$ for the remainder of the present text. The other thermodynamic parameters of activation can be calculated by Eyring equation [54]:

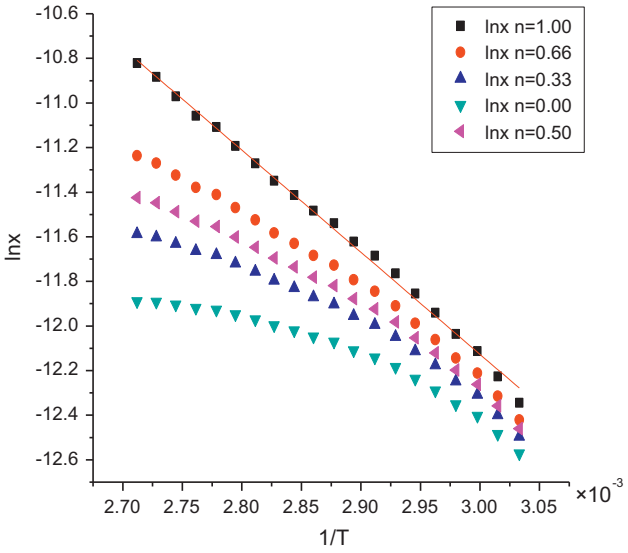

Fig. 3. Coats–Redfern plot of first degradation step for $[Zn_2(HAPC)(OAc)_3(H_2O)_3](H_2O)_3$ complex.

$$\Delta H = E - RT \quad (3)$$

$$\Delta S = R\ln\frac{hA}{k_B T} \quad (4)$$

$$\Delta G = \Delta H - T\Delta S \quad (5)$$

Thermodynamic parameters such as activation energy (E), pre-exponential factor (A), entropy of activation (ΔS), enthalpy of activation (ΔH) and free energy of activation (ΔG) of decomposition

Table 5
Kinetic parameters evaluated by Horowitz–Metzger equation for H_2APC complexes.

Complex	Peak	Mid temp (K)	E_a (kJ/mol)	A (S^{-1})	ΔH^* (kJ/mol)	ΔS^* (kJ/mol K)	ΔG^* (kJ/mol)
$[Zn_2(HAPC)(OAc)_3(H_2O)_3](H_2O)_3$	1st	349.22	43.94	4.91×10^4	41.04	−0.1564	95.66
	2nd	427.14	13.19	6.15×10^{-2}	9.64	−0.2711	125.43
	3rd	11.581	113.94	1.07×10^8	109.11	−0.0967	165.31
	4th	712.02	49.53	1.48×10^1	43.61	−0.2298	207.20
	5th	842.07	179.08	6.31×10^8	172.08	−0.0851	243.72
$[Cd(H_2APC)Cl_2]$	1st	553.37	179.53	1.55×10^{15}	174.93	0.0408	152.37
	2nd	657.46	105.99	3.40×10^6	100.53	−0.1265	183.67
	3rd	728.06	153.13	5.04×10^8	147.08	−0.0857	209.50
	4th	854.14	217.57	2.78×10^{11}	210.47	−0.0346	240.02

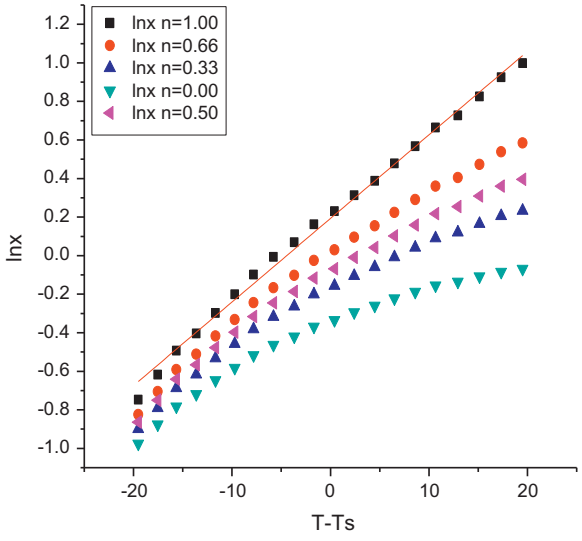

Fig. 4. Horowitz–Metzger plot of first degradation step for $[Zn_2(HAPC)(OAc)_3(H_2O)_3](H_2O)_3$ complex.

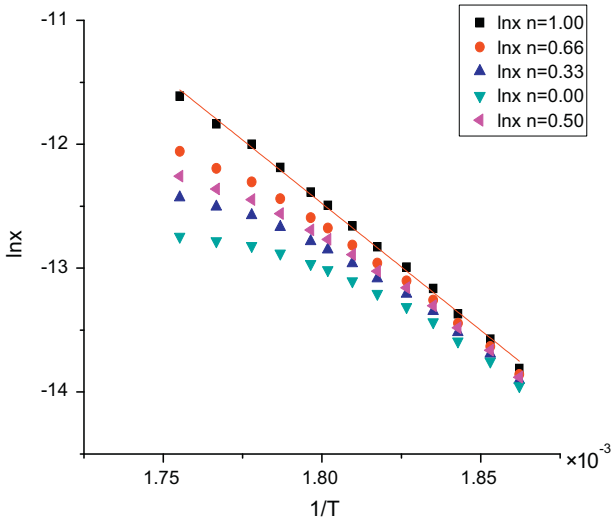

Fig. 5. Coats–Redfern plot of first degradation step for $[Cd(H_2APC)Cl_2]$ complex.

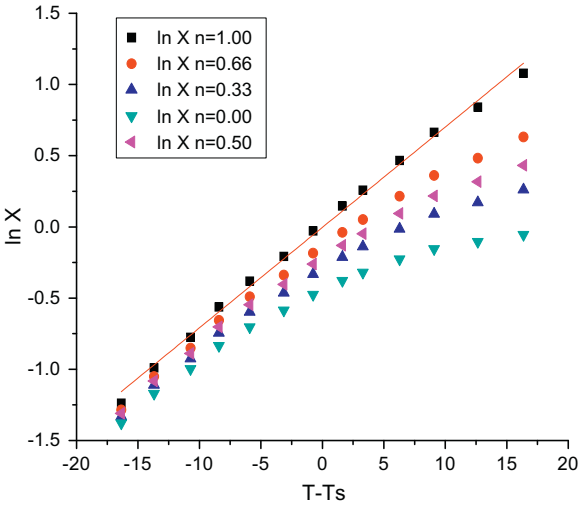

Fig. 6. Horowitz–Metzger plot of first degradation step for $[Cd(H_2APC)Cl_2]$ complex.

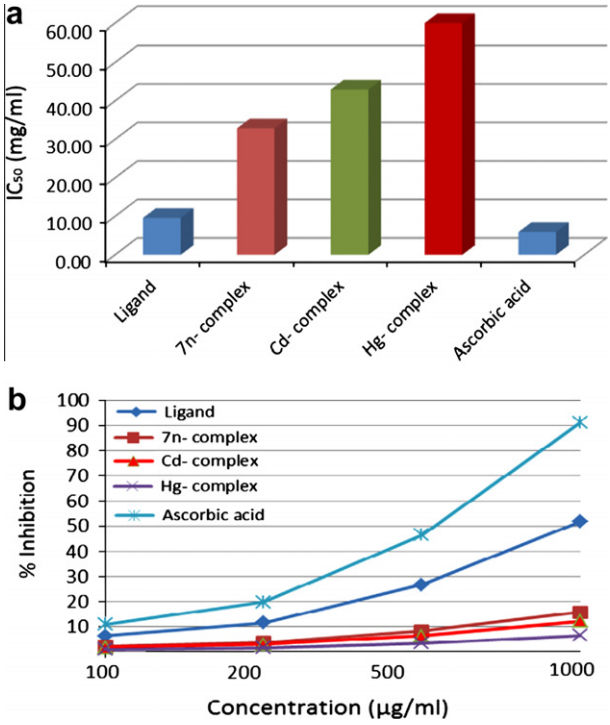

Fig. 7. DPPH inhibition of H_2APC and its metal complexes. (a) DPPH scavenging capacities (IC_{50}) of H_2APC and its metal complexes. (b) DPPH scavenging activity spectrophotometric assay of various concentration of H_2APC and its complexes.

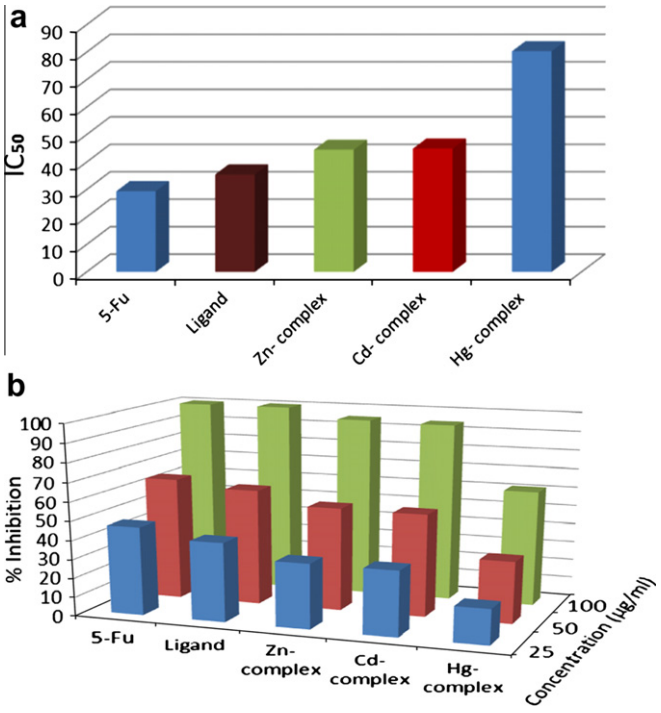

Fig. 8. Ehrlich in vitro assay for H_2APC and its complexes. (a) Ehrlich scavenging capacities (IC_{50}) of H_2APC and its metal complexes. (b) Ehrlich scavenging activity spectrophotometric assay of various concentration of H_2APC and its complexes.

steps were calculated using Coats–Redfern [50] and Horowitz–Metzger [51] methods (Tables 4 and 5). In both methods, the lift side of Eqs. (3) and (4) are plotted against $1/T$ and θ, respectively (Figs. 3–6). From the results, the following remarks can be pointed out:

Table 6
Antioxidant erythrocyte hemolysis assay for the prepared ligand and its metal complexes.

Compound	ABTS inhibition (%)	Erythrocyte hemolysis (%)
L-ascorbic acid[a]	96.57	4.08
H_2APC	53.90	4.48
Zn-complex	18.09	5.17
Cd-complex	12.76	4.48
Hg-complex	9.71	31.15

[a] Standard drug.

i) The high values of the energy of activation, E_a of the complexes reveals the high stability of such chelates due to their covalent bond character [55] and the increase of E_a on going from Zn(II) complex to Cd(II) complex reflects the greater thermal stability of first complex than the second one as E_a depends on the strength of (O → M ← N) and increases with increasing the cation radius.
ii) The positive sign of ΔG for the investigated complexes reveals that the free energy of the final residue is higher than that of the initial compound, and all the decomposition steps are non-spontaneous processes. Also, the values of the activation, ΔG increases significantly for the subsequent decomposition stages of a given complex. This is due to increasing the values of $T\Delta S$ significantly from one step to another which overrides the values of ΔH [56–58].
iii) The negative values of ΔS for the degradation process indicates more ordered activated complex than the reactants or the reaction is slow [54].

3.7. Biological application

3.7.1. Antioxidant activity

3.7.1.1. DPPH free radical scavenging activity. We found that most of compounds showed considerable free radical-scavenging activities (Fig. 7a). H_2APC was the strongest radical scavenger among the studied compounds with IC_{50} 9.64 mg/ml comparable with ascorbic acid (standard antioxidant). Zn(II) and Cd(II) complexes showed moderate scavenging activity with IC_{50} 32.88 and 42.97 mg/ml, respectively. On the other hand, Hg(II) complex exhibited no activity. The variation of % DPPH radical scavenging activity with concentration of test compounds is represented in Fig. 7b.

3.7.1.2. Antioxidant activity using ABTS inhibition and erythrocyte hemolysis. All compounds were tested for antioxidant activity using ABTS assay and rate erythrocyte hemolysis (Table 6). An inspection of the data in the table indicates that H_2APC exhibits the potent anti-oxidative activity. On the other hand, Zn(II) and Cd(II) complexes showed moderate activity while Hg(II) complex exhibited very weak or no antioxidant activity. With respect to erythrocyte hemolysis, the compounds can be arranged in the sequence: H_2APC = Cd(II) complex > Zn(II) complex > Hg(II) complex.

3.7.2. Antitumor activity using in vitro Ehrlich ascites assay

The compounds were screened for their antitumor activity (Fig. 8a). H_2APC showed the highest cytotoxic activity (61.41%) comparable to 5-furacil (standard drug) followed by Zn(II) and Cd(II) complexes. Hg(II) complex exhibited no cytotoxic activity. The variation of % inhibition of Ehrlich antitumor activity with concentration of test compounds is shown in Fig. 8b.

3.7.3. Structure activity relationship (SAR)

The antioxidant, erythrocyte hemolysis and antitumor activities of the investigated compounds is due to the presence of:

i. One C=O, two $(C{=}N)_{azomethine}$, one NH and two $(C{=}N)_{pyridine}$ groups free in the carbohydrazone, H_2APC moitey. So, it showed the potent antioxidant activity [59].
ii. In Cd(II) complex, there are still four donor sites free i.e. two $(C{=}N)_{pyridine}$ and two NH groups that can donate an electron or hydrogen radical thus be converted into a stable diamagnetic molecule [60].
iii. In case of the binuclear Zn(II) complex, there is only one NH group free. However its moderate activity can be referred to the presence of three acetate groups which enhances the scavenging activity.
iv. In Hg(II) complex showed no activity owing to its well known high toxicity although it most of the donor sites free otherwise C=O group.

4. Conclusion

1,5-Bis(1-(pyridin-2-yl)ethylidene)carbonohydrazide (H_2APC) and its mono- and binuclear complexes with Zn acetate, Cd(II) and Hg(II) chlorides were prepared. The complexes have been characterized and assigned the formulae $[Zn_2(HAPC)(OAc)_3(H_2O)_3]\cdot 3H_2O$, $[Cd(H_2APC)Cl_2]$ and $[Hg_2(H_2APC)_2Cl_4]$. A trigonal bipyramidal was proposed for Cd(II)complex, an octahedral for Zn(II) complex and a tetrahedral geometries, respectively. The ligand and its complexes were screened for antioxidant activity (using DPPH and $ABTS^+$), erythrocyte hemolysis and in vitro Ehrlich ascites assay. The relation between the structure of the studied compounds and their activity was discussed. All the data obtained revealed the high activity of Cd(II) and Zn(II) complexes and very weak activity for Hg(II) complex.

Appendix A. Supplementary material

Supplementary data associated with this article can be found, in the online version, at http://dx.doi.org/10.1016/j.molstruc.2012.04.029.

References

[1] G. Wilkinson, R.D. Gillard, J.A. McCleverty, Comprehensive Coordination Chemistry, vol. 2, Elsevier, Oxford, 1987.
[2] Yan Wang, Zheng Yin Yang, Bao-dui Wang, Trans. Met. Chem. 30 (2005) 879–883.
[3] D.W. Margerum, G.D. Owens, H. Sigel, Metal Ions in Biological Systems, vol. 12, Marcel Dekker Inc., New York, 1981. 75.
[4] J. Chakraborty, B. Samanta, G. Pilet, S. Mitra, Struct. Chem. 17 (6) (2006) 585–593.
[5] A. Shrivastav, N.K. Singh, P. Tripathi, et al., Biochimie 88 (9) (2006) 1209–1216.
[6] Z.H. Chohan, H. Pervez, K.M. Khan, C.T. Supuran, J. Enzyme Inhib. Med. Chem. 20 (1) (2005) 81–89.
[7] H.-J. Cristau, P.P. Cellier, J.-F. Spindler, M. Taillefer, Eur. J. Org. Chem. 4 (2004) 695–709.
[8] G.F. de Sousa, M.B.P. Mangas, R.H.P. Francisco, M.T. do P. Gambardella, A.M.G.D. Rodrigues, A. Barras, J. Braz. Chem. Soc. 10 (3) (1999) 222–230.
[9] A. Bacchi, G. Pelizzi, D. Jeremić, D. Sladić, M. Gruden-Pavlović, K. Andjelković, Trans. Met. Chem. 28 (2003) 935–938.
[10] C. Pelizzi, G. Pelizzi, G. Predieri, J. Organometal. Chem. 263 (1984) 9–20.
[11] D. Wester, G.J. Palenik, Inorg. Chem. 15 (1976) 755–761.
[12] A. Bino, R. Frim, M.V. Genderen, Inorg. Chim. Acta 127 (1987) 95–101.
[13] M. Mohan, P. Sharma, N.K. Jha, Inorg. Chim. Acta 107 (1985) 91–95.
[14] D. Wester, G.J. Palenik, J. Am. Chem. Soc. 95 (1973) 6505–6506.
[15] C. Aliage, E.A. Lissi, Int. J. Chem. Kinet. 30 (1998) 565–570.
[16] M. Cuendet, K. Hostettmann, O. Potterat, W. Dyatmiko, Helv. Chim. Acta 80 (1997) 1144–1152.
[17] M. Burits, F. Bucar, Phytother. Res. 14 (2000) 323–328.
[18] E.A. Lissi, B. Modak, R. Torres, J. Escobar, A. Urzua, Free Radical Res. 30 (1999) 471–477.
[19] A.B.A. El-Gazzar, M.M. Youssef, A.M.S. Youssef, A.A. Abu-Hashem, F.A. Badria, Eur. J. Med. Chem. 44 (2009) 609–624.
[20] R. Aeschbach, J. Loliger, B.C. Scott, A. Murcia, J. Butler, B. Halliwell, O.I. Aruoma, Food Chem. Toxicol. 32 (1994) 31–36.
[21] Y. Morimoto, K. Tanaka, Y. Iwakiri, S. Tokuhiro, S. Fukushima, Y. Takeuchi, Biol. Pharm. Bull. 18 (1995) 1417–1422.
[22] A.A. Fadda, F.A. Badria, K.M. El-Attar, Med. Chem. Res. 19 (2010) 413–430.

[23] A. El-Shafei, A.A. Fadda, A.M. Khalil, T.A.E. Ameen, F.A. Badria, Bioorg. Med. Chem. 17 (2009) 5096–5105.
[24] (i) B. Delley, J. Chem. Phys. 92 (1990) 508–517;;
(ii) B. Delley, Int. J. Quantum Chem. 69 (1998) 423–433;;
(iii) B. Delley, J. Chem. Phys. 113 (2000) 7756–7764;;
(iv) X. Wu ana, A.K. Ray, Phys. Rev. B 65 (2002) 85403–85409;;
(v) A. Kessi, B. Delley, Int. J. Quantum Chem. 68 (1998) 135–144.
[25] Materials Studio v 5.0 Copyright 2009. Accelrys Software Inc.
[26] W.J. Hehre, L. Radom, P.V.R. Schleyer, J.A. Pople, Ab Initio Molecular Orbital Theory, John Wiley, New York, 1986.
[27] B. Hammer, L.B. Hansen, J.K. Nørskov, Phys. Rev. B 59 (1999) 7413–7421.
[28] A. Matveev, M. Staufer, M. Mayer, N. Rösch, Int. J. Quantum Chem. 75 (1999) 863–873.
[29] W.J. Geary, Coord. Chem. Rev. 7 (1971) 81–122.
[30] O.A. El-Gammal, Spectrochim. Acta 75 (A) (2010) 533–542.
[31] D.X. West, J.K. Swearingen, J. Valdés-Martinez, S. Hernández-Ortega, A.K. El-Sawaf, F.V. Meurs, A. Castiñeiras, I. Garcia, E. Bermejo, Polyhedron 18 (1999) 2919–2929.
[32] A.A.R. Despaigne, J.G. Da Silva, A.C.M. Do Carmo, O.E. Piro, E.E. Castellano, H. Beraldo, J. Mol. Struct. 920 (2009) 97–102.
[33] S. Sagdinc, B. Koksoy, F. Kandemirli, S.H. Bayari, J. Mol. Struct. 917 (2009) 63–70.
[34] A.A.R. Despaigne, J.G. Da Silva, A.C.M. Do Carmo, F. Sives, O.E. Piro, E.E. Castellano, H. Beraldo, Polyhedron 28 (2009) 3797–3803.
[35] S.Y. Chundak, V.M. Leovac, D.Z. Obadović, D.M. Petrović, Transition Met. Chem. 11 (1986) 308–312.
[36] S.P. Perlepes, D. Kovala-Demertzi, S. Skaribas, D. Nicholls, S. Paraskevas, Thermochim. Acta 147 (1989) 153–174.
[37] T.H. Rakha, M.M. Bekheit, Chem. Pharm. Bull. 48 (2000) 914–919.
[38] D.P. Madam, M.M. da Mota, S.M. Nelson, J. Chem. Soc., A (1970) 90–794.
[39] D.P. Madden, S.M. Nelson, J. Chem. Soc., A (1968) 2342–2348.
[40] T.H. Rakha, Synth. React. Inorg. Met.-Org. Chem. 30 (2000) 205–224.
[41] U. El-Ayaan, G.A. EL-Reash, I.M. Kenawy, Synth. React. Inorg. Met.-Org. Chem. 33 (2003) 27–342.
[42] S. Chandra, A.K. Sharma, Spectrochim. Acta 72 (A) (2009) 851–857.
[43] K. Chandra, R.K. Sharma, B.S. Garg, R.P. Singh, J. Inorg. Nucl. Chem. 42 (1980) 187–193.
[44] F.A. El-Saied, A.M. Donia, S.M. Hamza, Thermochim. Acta 189 (1991) 297–311.
[45] R.C. Maurya, D.D. Mishra, S.K. Jaiswal, J. Dubey, Synth. React. Inorg. Met.-Org. Chem. 25 (1995) 521–535.
[46] A.N. Speca, N.M. Karayannis, L.L. Pytlewski, Inorg. Chim. Acta 9 (1974) 87–93.
[47] B. Beecroft, M.J.M. Campbell, R. Grzeskowiak, J. Inorg. Nucl. Chem. 36 (1974) 55–59.
[48] T.R. Todorović, U. Rychlewska, B. Warźajtis, D.D. Radanović, N.R. Filipović, I.A. Pajić, D.M. Sladic, K.K. Andelković, Polyhedron 28 (2009) 2397–2402.
[49] A. Bacchi, A. Bonini, M. Carcelli, F. Ferraro, E. Leporati, C. Pelizzi, G. Pelizzi, J. Chem. Soc., Dalton Trans. (1996) 2699–2704.
[50] I.A. Tossidis, C.A. Bolos, P.N. Aslanidis, G.A. Katsoulos, Inorg. Chim. Acta 133 (1987) 275–280.
[51] A.W. Coats, J.P. Redfern, Nature 201 (1964) 68–69.
[52] H.H. Horowitz, G. Metzger, Anal. Chem. 25 (1963) 1464–1468.
[53] A. Broido, J. Polym. Sci. A-2 (1969) 1761–1773.
[54] A.A. Frost, R.G. Pearson, Kinetics and Mechanism, John Wiley, New York, 1961.
[55] T. Hatakeyama, F.X. Quinn, Thermal Analysis Fundamentals and Applications to Polymer Science, second ed., John Wiley and Sons, Chichester, 1994.
[56] P.B. Maravalli, T.R. Goudar, Thermochim. Acta 325 (1999) 35–41.
[57] K.K.M. Yusuff, R. Sreekala, Thermochim. Acta 159 (1990) 357–368.
[58] S.S. Kandil, G.B. El-Hefnawy, E.A. Baker, Thermochim. Acta 414 (2004) 105–113.
[59] M-Hsiu Shih, Fang-Y. Ke, Bioorg. Med. Chem. 12 (2004) 4633–4643.
[60] B.F. Abdel-Wahab, G.E.A. Awad, F.A. Badria, Eur. J. Med. Chem. 46 (2011) 1505–1511.